COBEM 2023 27TH INTERNATIONAL CONGRESS OF MECHANICAL ENGENEERING

ABCM Brazilian Society of Mechanical Sciences and Engineering
27th ABCM International Congress of Mechanical Engineering
December 04-08, 2023, Florianópolis-SC, Brazil

COB-2023-0966

NUMERICAL ANALYSIS FOR THE DEVELOPMENT OF HIGH-LIFT LOW REYNOLDS NUMBER AIRFOILS USING INVERSE DESIGN GEOMETRIC MODIFICATIONS

João Victor Lopes Marchiori
Ayrton Cavallini Zotelle
Renato do Nascimento Siqueira
GPMF, Department of Mechanical Engineering, Instituto Federal do Espírito Santo - Campus São Mateus, Rod. BR 101 norte, km 58, Litorâneo, São Mateus - ES, 29932-540, Brazil
joaovictor.marchiori@hotmail.com
ayrton.zotelle@ifes.edu.br
renatons@ifes.edu.br

Abstract. *In the last decades, the development of Unmanned Aerial Vehicles (UAV) was accentuated all over the world, due to the lower cost, reduced size, as well as the absence of a crew. The operating conditions of UAVs typically involve low Reynolds, limiting aspects such as load capacity and also providing complexities such as extensive transition zones. A way to increase load capacity and decrease the runway length for landing and takeoff is by a higher lift coefficient. The present study proposes the development of high-lift low Reynolds airfoils, using as a basis the inverse design by potential flow theory and the widely used airfoil S1223, aiming to increase lift without compromising stall. The inverse design was carried out maximizing the pressure distribution around the airfoil and controlling the transition, obtaining the geometry as an output. The aerodynamic verification was carried out by CFD technique using two-dimensional simulations with the Spalart-Allmaras turbulence model. Furthermore, three-dimensional simulations were carried out with a hybrid URANS/LES turbulence model combined with Transition SST. Two high-lift low Reynolds airfoils were developed, with lift gains up to 15% despite an increase drag is associated. It was observed that the transition significantly influences in the prediction of aerodynamic coefficients, in particular the drag coefficient, besides to the three-dimensional methodology and URANS/LES model having shown greater capacity for predicting the region stall and maximum lift coefficient. It was shown that the design philosophy was successful and that the inverse design combined with the CFD technique for prediction of aerodynamic coefficients can be a powerful tool for airfoil development.*

Keywords: *Low Reynolds Airfoils, High-Lift Airfoil, Inverse Design, UAV, Airfoil Design.*

1. INTRODUCTION

In recent decades, aircraft manufacturing has not been limited to commercial aircraft, but attention was also given to the Unmanned Aerial Vehicles (UAVs). The UAVs have attracted interest because of their advantages, such as high versatility in maneuvers, long-term operations (eliminating the problematic of human fatigue), reduced size, lower manufacturing cost and the absence of crew, which allows operation even under high-risk conditions. The current usage of drones is numerous, ranging from the military to the civil sector (de Medeiros Neto, 2016).

The operational conditions of UAVs motivate the elaboration of studies dedicated to the development and analysis of airfoils specifically designed to achieve high lift at low Reynolds (typically 2×10^5 to 5×10^5), as shown by Selig and Guglielmo (1997) in the design of the S1223 airfoil. The development of high-lift airfoils allows obtaining many benefits: lower flight velocities, greater payload and smaller runway lengths for takeoff and landing (Selig and Guglielmo, 1997). As discussed by Ashby (1996) in NASA Technical Memorandum 110432, for a given payload, the takeoff, and landing distances are defined by high lift characteristics. Besides, higher lift coefficients allow smaller wing areas to meet the landing and takeoff requirements (Morgan and Ferris, 1987). Currently, there are software programs such as XFLR5 designed to evaluate low Reynolds airfoils, allowing the use of the inverse design methodology based on potential flow theory, obtaining the geometry from the desired pressure distribution. Computational Fluid Dynamics (CFD) can be used to verify the design of airfoils, ensuring greater precision with transition models for low Reynolds aerodynamics and a more accurate representation of the stall with a hybrid URANS/LES models.

Over the decades, several classic studies have been carried out with the aim of maximizing the lift of airfoils operating at low Reynolds. A technique used in airfoil designs to control aerodynamic performance, such as mitigating the Laminar Separation Bubble (LSB) is the use of the transition ramp. As shown by Selig (2003), it is an instability introduced in the pressure gradient, which allows controlling the transition of the flow. One method to decrease separation bubble losses is to shift the transition upstream (leading edge direction), which would decrease the moment deficiency (Drela,

1988). The maximum lift challenge was approached by Liebeck (1978) from aircraft manufacturer McDonnell Douglas Corporation, proposing the maximization area under the V/V_∞ curve, which represents the distribution of inviscid velocity (or equivalently, the pressure distribution) around the airfoil. The author argues that it is necessary to use a Stratford-type pressure distribution, allowing the maximum pressure recovery in the shortest distance. Maximization is done by approximating the stagnation velocity $V \approx 0$ on the lower surface of the airfoil and increasing the velocity on the upper one $V \geq 0$. The design philosophy described above has some points to be highlighted. The Stratford pressure recovery is dangerous for separating bubbles, and also regarding the complete separation of the flow, which can cause stall with abrupt characteristics. The previous formulation is not optimal, being possible to obtain greater lift with a less concave pressure recovery than Stratford-type distributions (Eppler, 1990). This aspect contributes to the introduction of a gradual pressure gradient. Selig and Guglielmo (1997) and Eppler (1990) showed that there are some parameters that tend to increase the maximum lift coefficient $C_{l,max}$ of the airfoil, such as a higher moment coefficient $C_{m,c/4}$ and a concave pressure recovery surface, being the greater curvature beneficial for this purpose. However, it was found that the stall rate increases when more lift is needed. This shows how important it is to control the boundary layer.

Nowadays, research such as that by Nwokolo *et al.* (2023) studied the optimization of low Reynolds airfoils using NACA2408 and the inverse design methodology with the XFLR5 software, which uses the capabilities of XFOIL (Drela, 1989). It has been shown that there is still room for improvement in lift and, as a result, an airfoil with superior performance to the NACA 2408 was obtained, verifying with greater fidelity through the CFD technique and the Spalart-Allmaras model. A multi-objective optimization of low Reynolds airfoils using a generic algorithm and the Bezier curve was conducted (Wei *et al.*, 2020). The multi-objective optimization allowed a global optimization of the airfoil, keeping the drag similar to the Eppler 387 base profile and increasing lift and $C_{l,max}$. It was observed that the highest $C_{l,max}$ was obtained by a smaller adverse pressure gradient on the upper surface, which aided to postpone the flow separation.

A detailed analysis of geometric parameters was conducted in the optimization of NACA airfoils through the particle swarm technique using both XFOIL and CFD (Echavarria *et al.*, 2022). It was observed that CFD produced better results and that the greatest efficiencies were obtained with smaller curvatures, in addition to a linear relationship between the design lift coefficient and the maximum curvature. The optimization was applied to the S1223 airfoil, obtaining greater aerodynamic efficiencies in some regions, but with a significant reduction in lift in most of the curve. Similarly, it was carried out numerical simulations with the S1223 airfoil varying its thickness, using Ansys FLUENT® (Ma and Liu, 2009). It was observed that thicker airfoils had lower aerodynamic efficiency. On the other hand, the greater thickness favored the better stall behavior. Another research was conducted through single-objective and multi-objective optimization using the S1223 airfoil (Ma *et al.*, 2010). It was shown that the design challenge for low Reynolds airfoils is the optimization of the transition point, as this significantly affects frictional drag. The multi-objective optimization obtained lower aerodynamic efficiency than the single-objective one, but maintained the $C_{l,max}$ characteristics. Another study carried out the development of a new high lift airfoil (Cerra and Katz, 2008). It has been cited that the pressure gradient in the upper surface is essential to control the transition and flow separation. The development of high lift was based on maximizing pressure distribution, obtaining an airfoil with high lift and thickness. The behavior of a low Reynolds airfoil was studied using LES simulations and wind tunnel tests (Anyoji *et al.*, 2014). It has been observed that a flatter top surface aids in delaying flow separation and reducing pressure drag. It was also noted that a greater curvature increases lift.

The aerodynamic characteristics of low Reynolds airfoils have particularities, especially regarding the transition. Studies evaluated in a two-dimensional simulation the Spalart-Allmaras model, $k-\omega$ SST, and the Transition SST applied to the S1223 airfoil (Boughou *et al.*, 2022). The author reinforces the importance of the transition to low Reynolds airfoils, discussing the three-dimensional characteristic of laminar separation bubbles observed by other studies such as Wauters and Degroote (2018). It was concluded that the Spalart-Allmaras model predicts well in the pre-stall region in agreement with experiments, with the Transition SST better capturing the drag and the stall region. Based on the S1223, an in-depth analysis was performed, evaluating several turbulence models using Ansys FLUENT® (Hubbe, 2017). The work showed that the transition effects are not well captured by traditional RANS models, with the Transition SST achieving better results. Experiments were also carried out in a wind tunnel, showing that the LSB numerically predicted by the Transition SST reached good agreement with the experimental result.

There are several studies in the literature that evaluate the capabilities of the URANS/LES models for aerodynamic applications due to its attractiveness for saving computational cost using URANS models in the boundary layer and solving the largest structures in LES away from the wall. In this scope, a study evaluated in a three-dimensional simulation the Scale Adaptive Simulation (SAS) model for the NACA0021 airfoil at an angle of attack of 60° (Wang *et al.*, 2019). The study highlights the importance of a correct dimensionless time and a domain width of dimensions capable of representing turbulent structures. The authors show that several hybrid URANS/LES models have better predictions than URANS, both for mean magnitudes and for unstable turbulent structures. The blend between the Transition SST model and the Delayed Detached Eddy Simulation (DDES) was evaluated (Sa *et al.*, 2016). It was mentioned that, although URANS/LES models are suitable for complex external flows, they cannot capture the transition due to the URANS model being based on fully turbulent flow. The blend between URANS/LES and Transition SST allows simulating the unstable turbulent wake and also the laminar-turbulent transition in the boundary layer, such as the laminar separation bubble. Another study evaluated the

Shielded Detached Eddy Simulation (SDES) model in a three-dimensional and transient manner on a high thickness airfoil (Mereu *et al.*, 2019). It was concluded that the model has significantly superior capabilities for simulating stall compared to the RANS approach. The stall angle was captured with higher accuracy, as well as its mechanism and behavior.

Based on the cited works, it is evident that although the development of high-lift airfoils has been a topic addressed for decades, it still motivates recent research, especially driven by advances in UAV technology. Among the various studies, there is a lack of significant gains in lift, indicating that there is still room for further investigation. The studies that achieved the highest gains only used potential flow for verification, which can lead to significant discrepancies. In this regard, the combination of inverse design methodology using potential flow (lower computational cost) with three-dimensional CFD approaches for low Reynolds number aerodynamics verification using hybrid transition and LES models appears to be an alternative for the development of new low Reynolds airfoils, obtaining higher accuracy in the aerodynamic coefficients. In this context, the present work seeks to develop modified high-lift airfoils using the inverse design methodology and the S1223 airfoil in a single-objective optimization, increasing the lift coefficient and the maximum lift coefficient, maintaining the stall characteristics and evaluating the results numerically by CFD technique.

2. METHODOLOGY

2.1 Development of High-Lift airfoils

The airfoils were developed for a Reynolds $Re = 200,000$ and an angle of attack of 0°, ensuring that the modified airfoils were capable of operating under the typical lower Reynolds condition of UAVs and maintain good characteristics close to cruise operation. Additionally, this is the design Reynolds number for the S1223 (Selig and Guglielmo, 1997). The development of the high-lift airfoils primarily followed the inverse design airfoil methodology to maximize pressure distribution. For this purpose, the S1223 was used as a base, and the XFLR5 software was employed, specifically developed for low Reynolds number airfoil analysis, allowing to obtain the geometry by the pressure distribution. Control points were added to define the shape and magnitude of the curve. The general methodology involved a single-objective optimization with the following requirements: increasing the lift coefficient and $C_{l,max}$; maintaining stall characteristics similar to the S1223 profile, avoiding abrupt stall; preventing flow separation on the lower surface at slightly negative angles.

The increase in lift was based on the design philosophy proposed by Liebeck (1978) and Eppler (1990), where the inviscid flow velocity around the airfoil was distributed in a way to reduce the velocity on the lower surface (approaching stagnation) and increase it on the upper surface, aiming to maximize the area under the V/V_∞ curve (Fig. 1). The pressure recovery was maintained concave with a gradual curvature (gradual adverse gradient) to maximize lift and mitigate the adverse effects of Stratford-like distributions, such as abrupt stall and large separation bubbles. The transition ramp was introduced with a smooth slope to facilitate flow transition without premature flow separation. In addition to increasing lift, these measures were taken to reduce the increase in stall rate associated with concave pressure recovery for the lift increment observed by Selig and Guglielmo (1997). The immediate geometric consequence resulting from all these procedures was a highly curved and thick airfoil. During the process, it was also necessary to modify the leading edge radius to prevent flow separation on the lower surface due to the increased curvature of the airfoils.

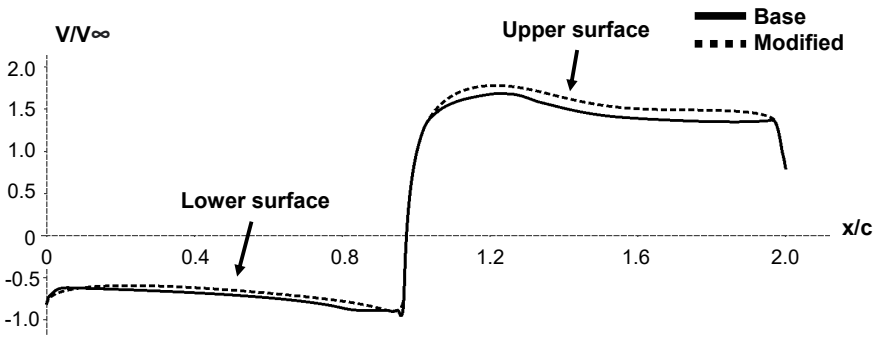

Figure 1: Methodology for increasing lift on airfoils.

In parallel with the lift increase process, the development of the airfoils considered the position of the transition ramp relative to the chord position to control the laminar-turbulent transition of the flow, as a transition upstream of the separation bubble can help mitigate its effects. On the other hand, a turbulent boundary layer tends to generate more drag due to friction. To evaluate the effects of the transition ramp position and, consequently, the pressure recovery position, the two airfoils were designed by displacing the transition ramp in opposite directions relative to the position of the base S1223 profile, as exemplified in Fig. 2. The displacement of the transition ramp at the leading edge was carried out to evaluate the potential reduction of the separation bubble and the hypothesis that the upstream transition of the flow and the highly energetic turbulent regime can help mitigate the stall rate. The displacement of the transition at the trailing edge

aimed to assess the results obtained from a shorter turbulent boundary layer. The two resulting profiles followed the same lift-increase procedure, differing only in the displacement of the transition ramp. The airfoils were named S1223 JVM01 (leading-edge ramp) and S1223 JVM02 (trailing-edge ramp), and their characteristics will be presented in the results.

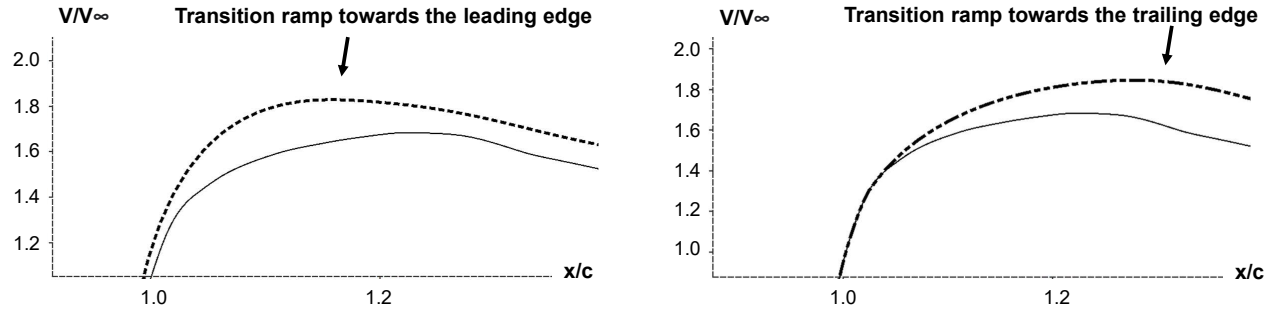

Figure 2: Displacement of the transition ramp and pressure recovery on the upper surface of the airfoil.

2.2 Methodology for Two-Dimensional and Three-Dimensional Simulation

To verify the aerodynamics of the resulting airfoils and also to verify the representativeness against the experimental data of the S1223, simulations using the CFD technique and commercial software Ansys FLUENT® were conducted, maintaining the same Reynolds design (Reynolds = 200,000 and far-field Mach = 0,0085) and varying the angle of attack. Figure 3 shows the geometries and their boundary conditions. The velocity was defined vectorially at the inlet, the pressure at the outlet was atmospheric, the condition of non-slip on the wall and the condition of periodicity on the lateral faces for the 3D case.

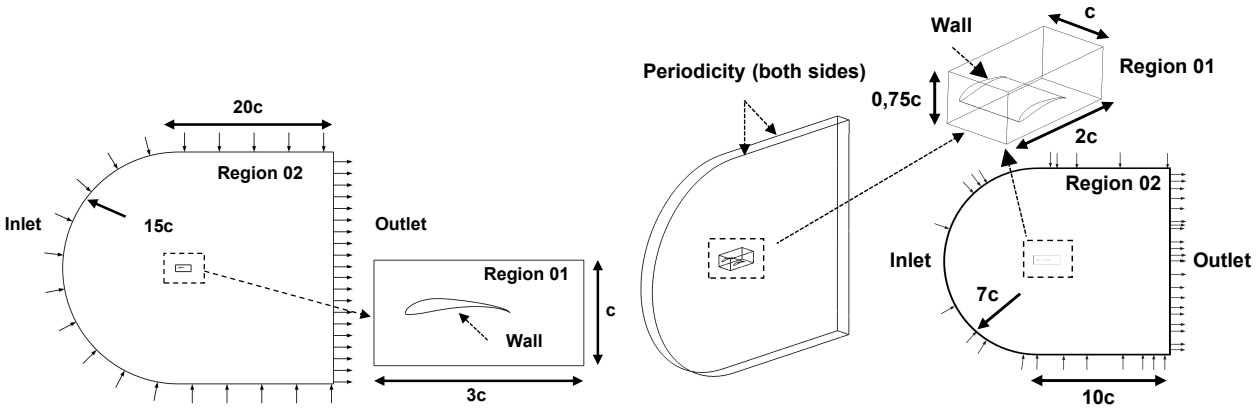

(a) 2D Geometry (b) 3D Geometry

Figure 3: Geometry and boundary conditions.

The 2D methodology (Fig. 3a) aimed to save computational cost during the evaluation of candidate airfoils, applying the widely used Spalart-Allmaras. The two best airfoils were subsequently evaluated using the 3D simulation methodology (Fig. 3b), to better represent intrinsically three-dimensional characteristics such as the complex turbulent flow in the stall region, its behavior (smooth or abrupt) and the value of $C_{l,max}$. The regions 01 of each geometry have a greater refinement to ensure better representativeness of the turbulent wake in the stall and, using the URANS/LES Shielded Detached Eddy Simulation (SDES) model for the 3D simulations, to control the resolution of the turbulent scales by the cutoff wavelength. To ensure that at least 80% of the turbulent kinetic energy is effectively resolved in the wake region, the cutoff length for LES can be obtained by the relation $kL \approx 38$ where L is the integral length of the turbulence and k the wave number, resulting in a size of element of $l_c = 0.0165c$ for the 3D case (Solís-Gallego *et al.*, 2020). A length of $l_c = 0.005c$ was used for the 2D case. The regions 2 far from the zone of interest allowed larger elements of sizes $0.5c$ for both approaches. For all cases, was defined a value of $y^+ = 0.5$ sufficient for the laminar sublayer and a turbulence length of $0.1c$ at the entrance with turbulence intensity of 1%, usually present in wind tunnels (Hubbe, 2017).

The solution algorithms, physical parameters, turbulence models used, and the respective methodology are summarized in Tab. 1. The simulations were conducted transiently for a Flow Through number of 15, reaching the steady state. The dimensionless time step for the Transition SST - SDES model was taken as sufficient to maintain $CFL < 1$ in the turbulent wake and an adequate cutoff frequency for LES (Menter, 2015; Mereu *et al.*, 2019; Wang *et al.*, 2019). It was observed that the discretization and interpolation schemes need to be of second order for the correct description of the LSB. The

turbulence variables for the three models used second-order schemes. The simulated cases for the 2D methodology ranged from: -2° to 14° with 2° intervals. For a representation of the non-linear behavior close to the stall region, angles of 13° and 15° were also simulated. For the S1223, an angle of 16° was additionally simulated. In the 3D methodology, to reach the level of detail necessary for a better representation of the stall, the hybrid URANS/LES SDES model was used. The 3D simulations were conducted using the Transition SST model in the linear region of the C_l versus α curve and the hybrid blend model Transition SST - SDES in the stall region. For presentation of results, the nomenclature Transition SST - SDES to refer to this methodology. The angle of attack for cases simulated with Transition SST were from 0° to 12° with increments of 3°, additionally simulating the angle of -2°, and for Transition SST - SDES were from 14° to 18°, with 2° intervals. For all cases, the steady state for obtaining the data was confirmed by the stabilization of the Cl curve over time. To define the total simulation time and ensure that a steady state condition was reached in all cases, a Flow Through (FT) value of 15 was chosen. This value represents the number of times the fluid passes through the chord of the airfoil.

Table 1: Solution algorithms, physical parameters and turbulence models used for each methodology.

Methodology		2D	3D	
Turbulence Models		Spalart-Allmaras	Transition SST	Transition SST - SDES
Dimensionless time-step, $t^* = V_\infty t/c$		0.026	0.04	0.01
CFL		25	≈ 2	< 1
Pressure-velocity coupling		Coupled	SIMPLEC	SIMPLEC
Spacial discretization	Gradient	Least Squares Cell Based		
	Momentum	Second Order Upwind	Second Order Upwind	Bounded Central Differencing
	Pressure	Second Order		
Flux Type		Rhie-Chow: distance-based		
Transient Formulation		Second Order Implicit		Bounded Second Order Implicit

2.3 Mathematical formulation

The Direct Numerical Simulation (DNS) capable of predicting all scales of turbulence requires a prohibitive computational cost for most applications. To apply methodologies such as URANS and URANS/LES, the Navier-Stokes and continuity equations are filtered, allowing the resolution of the part of the turbulent spectrum associated with larger scales, while smaller scales are modeled. In the URANS approach practically the entire spectrum is modeled, while in the LES the structures are directly resolved up to the grid limit, with sub-grid stresses being modeled (Mereu *et al.*, 2019; da Silveira Neto, 2020). The value of the property is decomposed into the filtered/resolved field $\overline{\phi}(\mathbf{x}, t)$ and the fluctuation sub-grid of this quantity $\phi'(\mathbf{x}, t)$, which results $\phi(\mathbf{x}, t) = \overline{\phi}(\mathbf{x}, t) + \phi'(\mathbf{x}, t)$. Spatial filtering is defined by Eq. (1) where G is the filter function that defines the spectrum cutoff. An analogous procedure is done for temporal filtering.

$$\overline{\phi}(\mathbf{x}) = \int_{-\infty}^{\infty} G(\mathbf{x} - \mathbf{x}')\phi(\mathbf{x}')d\mathbf{x}'. \tag{1}$$

Performing the filtering of the Navier-Stokes and continuity equations for an incompressible flow and replacing the decomposition, the equations of the present study are obtained:

$$\nabla \cdot \overline{\mathbf{u}} = 0\,, \tag{2}$$

$$\frac{\partial \overline{\mathbf{u}}}{\partial t} + \nabla \cdot (\overline{\mathbf{u}}\,\overline{\mathbf{u}}) = -\frac{\nabla \overline{p}}{\rho} + \nabla \cdot \left[(\nu + \nu_t)(\nabla \overline{\mathbf{u}} + \nabla \overline{\mathbf{u}}^T) - \frac{2}{3}k\overline{\overline{I}}\right], \tag{3}$$

in which k is the turbulent kinetic energy, $\overline{\overline{I}}$ is the identity tensor and ν_t is the turbulent kinematic viscosity. The sub-grid stress tensor $\overline{\overline{\tau}}^{LES} \equiv \overline{\mathbf{u}\,\mathbf{u}} - \overline{\mathbf{u}}\,\overline{\mathbf{u}}$ due to the filtering process was replaced by the hypothesis of Boussinesq $-\overline{\overline{\tau}} = \nu_t(\nabla \overline{\mathbf{u}} + \nabla \overline{\mathbf{u}}^T) - \frac{2}{3}k\overline{\overline{I}}$. For the closure of the system, the calculation of the kinematic viscosity is carried out by the evaluated one-equation Spalart-Allmaras, four-equation Transition SST and Transition SST - SDES turbulence models. In the SDES model, the turbulent viscosity is calculated by a sub-grid model like the Smagorinsky one, allowing scale adaptation. Details about the models can be obtained from Menter (2015) and Ansys (2021) .

3. RESULTS

3.1 Developed high-lift low Reynolds airfoils

The development of the modifications for increased lift resulted in two airfoils, named S1223 JVM01 for the case where the transition ramp was displaced towards the leading edge, and S1223 JVM02 for the case where the transition ramp was

displaced towards the trailing edge. The resulting airfoils and the base S1223 airfoil are illustrated in Fig. 4, with the geometric configurations summarized. The geometric consequence of the inverse design philosophy was the achievement of airfoils with higher curvature and also a higher moment coefficient, in accordance with the trend for increased lift observed by Selig and Guglielmo (1997). The geometric result of the transition ramp displacement was obtained as expected, with the airfoil that has the transition ramp displaced towards the leading edge (S1223 JVM01) resulting in a steeper geometric inclination of the upper surface near the leading edge.

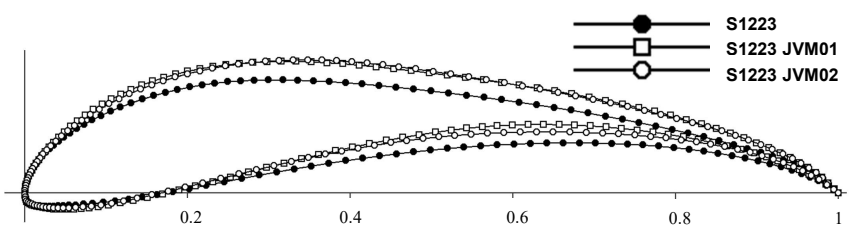

Airfoil	Curvature	Thickness
S1223	8.67%	11.93%
S1223 JVM01	10.78%	13.98%
S1223 JVM02	10.62%	13.50%

Figure 4: Developed high-lift low Reynolds airfoils and the S1223.

The increasing of the radius of the leading edge was necessary to prevent boundary layer separation at negative or small angles of attack. This procedure reduced efficiency but was deemed necessary for flight safety at low angles. It was noticed that curvature alone was not the only one determining parameter for increased lift, with the thickness playing an important role as well, allowing for a larger area under the inviscid velocity distribution curve, resulting in greater lift with a gradual concave pressure recovery in line with the philosophy discussed by Eppler (1990). During the development process, it was also observed that increased thickness helped delay stall and provided a smoother behavior. The direct relationship between the moment coefficient and the lift gain was observed, as shown by Selig and Guglielmo (1997) and Eppler (1990).

3.2 Comparison of turbulence models against experimental data from the literature

For the 2D and 3D simulations, the obtained results of the S1223 airfoil were compared with the experimental data available in the literature from the wind tunnel at the University of Illinois at Urbana-Champaign (UIUC) (Selig and Guglielmo, 1997; Selig *et al.*, 1995). The Fig. 5a illustrates the comparison between the Spalart-Allmaras 2D model and the Transition SST - SDES 3D model. It can be noted that both models accurately predict the lift coefficient in the linear region compared to the UIUC 1997. However, the Transition SST - SDES model combined with the 3D methodology achieved a much closer representation to the experimental data in the stall region, reaching a $C_{l,max} = 2.11$ with a deviation of only 0.5% from UIUC 1995, while the Spalart-Allmaras model using the 2D methodology exhibited significant errors in the stall region. The stall angle was also better predicted by the 3D approach. The improved representation of the Transition SST - SDES model in the stall region is attributed to the better resolution of three-dimensional turbulent structures. The drag polar shown in the Fig. 5b also reveals good agreement between the models in predicting drag in the linear region, although the Transition SST - SDES model achieved better results, especially in the stall region. This is due to the improved performance of the transition model in modeling the boundary layer with the presence of a laminar separation bubble, which was not predicted by the Spalart-Allmaras model, in which no LSB were observed.

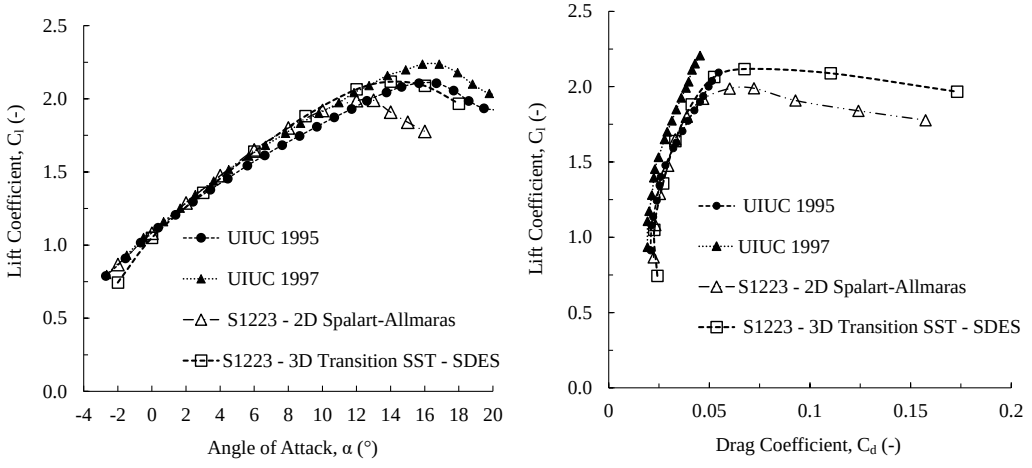

(a) Lift coefficient (b) Drag polar

Figure 5: Comparison of lift and drag coefficient using 2D and 3D methodologies against UIUC data.

The comparison of the airfoils using both modeling approaches is illustrated in Fig. 6. The Spalart-Allmaras model (Fig. 6a) predicted significant and uniform lift gains for the developed airfoils compared to the S1223, across the entire range of angles of attack, including the $C_{l,max}$. The developed airfoils exhibited very similar gains, differing only in the stall region, with the S1223 JVM01 profile having the same stall angle as the S1223. Looking at the comparison of the airfoils using the Transition SST - SDES model (Fig. 6b), again, lift gains are observed across the entire range, including the $C_{l,max}$. For the Spalart-Allmaras model, the average lift coefficient gains were 10.41% and 9.19% for S1223 JVM01 and JVM02, respectively, and for the Transition SST - SDES model, the gains were 8.79% and 8.81%. However, the differences in the stall region between the developed airfoils became more evident. The S1223 JVM02 airfoil showed a lower stall angle than the S1223, while the S1223 JVM01 maintained the same stall angle and behavior very similar to the S1223, which can be explained by the transition moving towards the leading edge due to the change in the transition ramp. On the other hand, the JVM02 airfoil showed a smoother C_l decrease after stall. The importance of controlling the pressure gradient in flow separation has been reported in previous studies, such as Cerra and Katz (2008). This aspect observed in both graphs shows that the change in the transition ramp can affect stall characteristics, with an early transition being beneficial for stall angle control. The significant differences between the models (URANS and URANS/LES) and methodologies 2D and 3D in predicting $C_{l,max}$ and stall behavior reinforce the need to consider these approaches in the development of airfoils.

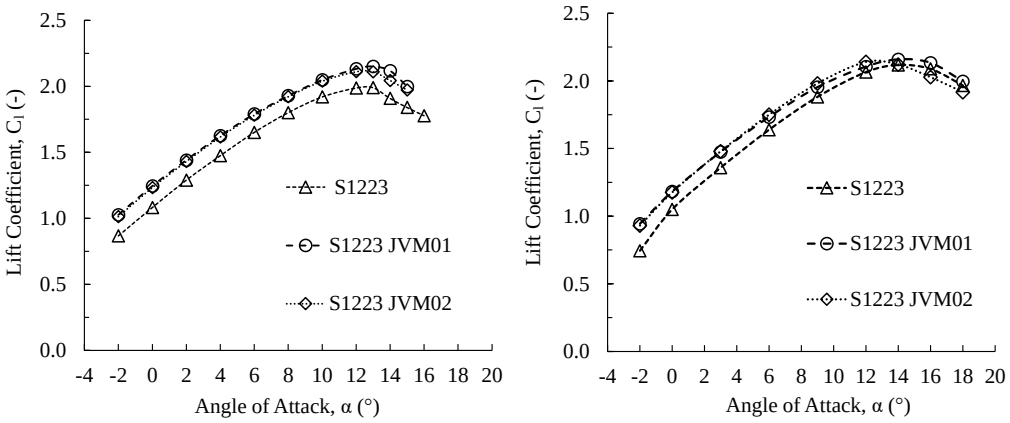

(a) 2D Spalart-Allmaras (b) 3D Transition SST - SDES

Figure 6: Comparison of lift coefficient for the airfoils.

The evaluation of drag and lift-to-drag ratio (Cl/Cd) for the airfoils is performed by the drag polar in Fig. 7. The Spalart-Allmaras model predicted a very similar lift-to-drag ratio for the developed airfoils compared to the S1223, with a slight decrease in efficiency for lower C_l values but equal or higher efficiency for higher C_l values associated with larger angles of attack. Both developed airfoils achieved almost identical drag with this model, with a small increase in drag compared to the S1223, on average less than 15% for both. On the other hand, significant differences were observed with the Transition SST - SDES model, with the S1223 JVM02 airfoil exhibiting significantly lower drag than the S1223 JVM01, and both airfoils experiencing a greater loss in efficiency compared to the S1223. This aspect highlights the insensitivity of the Spalart-Allmaras model to the transition induced by separation in the LSB, which can significantly affect drag prediction, even when the airfoils have different transition regions. The LSB was not observed in the Spalart-Allmaras. In contrast, the URANS Transition SST model used in the boundary layer better captured the impact of transition on drag.

Figure 8 shows the percentage variation of drag due to pressure (ΔC_p) and friction (ΔC_f) in relation to the S1223 airfoil. It can be observed that both models predicted significant increases in pressure drag, but the S1223 JVM02 profile produced lower drag. This result indicates that a substantial portion of the additional pressure drag is a direct consequence of the increased thickness and curvature. When comparing the prediction of ΔC_f in both models, it can be noted that the Spalart-Allmaras model exhibited virtually the same behavior for both airfoils, while the Transition SST - SDES model showed lower friction drag for the S1223 JVM02 airfoil compared to the S1223. These aspects reinforce the difficulty of the Spalart-Allmaras model in predicting drag and corroborate the expected shorter turbulent boundary layer of the S1223 JVM02, resulting from the displacement of the transition towards the trailing edge and reduction of drag. An accentuated increase in ΔC_p of the S1223 JVM02 in the stall region was observed in Fig. 8b, showing that the delayed transition can worsen the stall characteristics, despite producing lower drag in the rest of the operating range.

To assess the effects of inverse design on pressure and friction distribution using the Transition SST - SDES model, Fig. 9 was plotted. Figure 9a illustrates the coefficient of friction distribution on the upper surface, where the region of separation bubble with $Cf < 0$ indicating reverse flow can be visualized. The S1223 JVM01 airfoil has a separation bubble more towards the leading edge compared to the S1223 JVM02, justified by the displacement of the adverse pressure gradient. The transition induced by separation actually occurs upstream for the S1223 JVM01 airfoil, similar to the S1223, corroborating their similar stall characteristics. It is evident that the size of the separation bubble is very similar

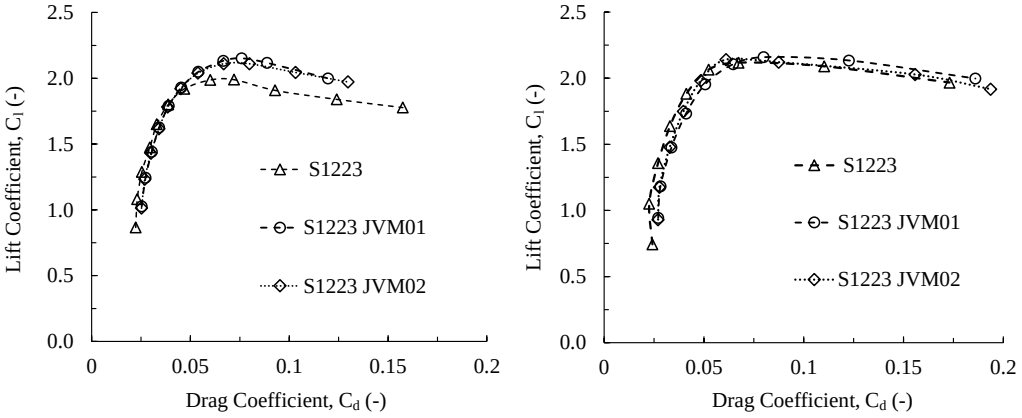

(a) 2D Spalart-Allmaras (b) 3D Transition SST - SDES

Figure 7: Comparison of drag polar for the airfoils.

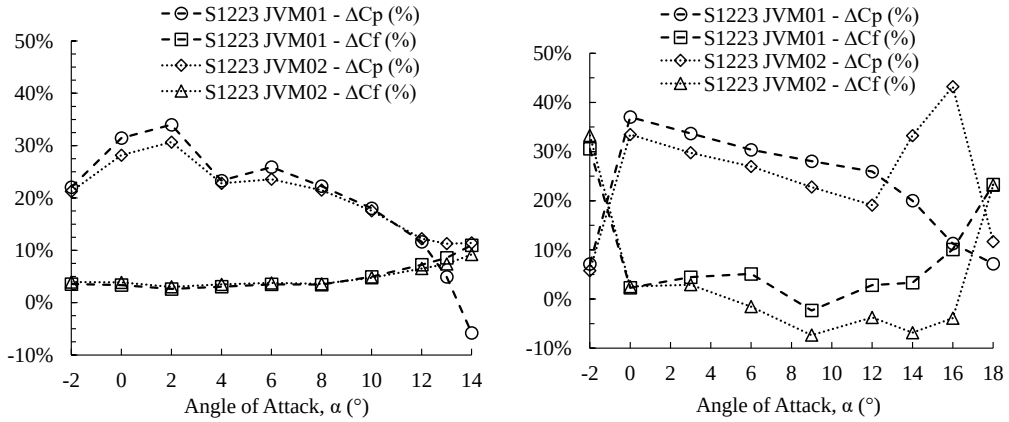

(a) 2D Spalart-Allmaras (b) 3D Transition SST - SDES

Figure 8: Comparison of the variation in pressure (ΔC_p) and friction (ΔC_f) drag relative to the S1223.

for all airfoils, with an equal average size of $l/c = 0.14$ between angles of attack from 0° to 12°, where l is the bubble length, although the position differs. This aspect indicates that the size of the bubble was not significantly affected by the modifications. The pressure distribution is shown in Fig. 9b, highlighting with arrows the regions of lift gain and loss. The resulting area inside the curve is greater for both airfoils, justifying the higher lift. The gains are significant in the upper region due to the increased thickness, while in the lower region, gains are mainly achieved through curvature. The higher aft load of the modified airfoils resulted in a higher moment coefficient, as observed for high-lift airfoils (Selig and Guglielmo, 1997). There is a loss on the lower surface near the leading edge due to the presence of a more impactful bubble in the developed airfoils. It can be noted that the transition ramp and adverse pressure gradient on the upper surface is similar among the three airfoils, especially for the S1223 JVM01 and S1223, which help explain their similar angle and stall characteristics. On the S1223 JVM02, the adverse pressure gradient occurs towards the trailing edge. Finally, it is worth noting that the losses in the upper bubble, proportional to ΔC_p (Drela, 1988), are similar for all three airfoils.

Finally, Fig. 10 illustrates the three airfoils in a stall condition using an isosurface of the Q-criterion with a velocity contour. Visually, the resolution of various turbulent scales and three-dimensional vortices was well represented by the hybrid URANS/LES model, ensuring a better representation of the stall. It can be observed that the large amount of turbulent structures generated by the boundary layer separation results in an intense turbulent wake, typical of the stall condition. It is noticeable that the wake is larger for the modified airfoils, which can be justified by the increased curvature. By observing the numerous three-dimensional structures, it becomes clear that predicting this condition in a two-dimensional simulation is challenging, justifying the better results obtained with the three-dimensional methodology compared to experiments. Close to the leading edge (zoom 01) can be seen the Tollmien-Schlichting waves and subsequent three-dimensional instabilities. With the SDES model, a natural transition was noted. This fact can be explained because the transition strongly depends on the free stream information (by the Transition SST), which is influenced by the SDES, explaining the change from the transition induced by a separation bubble to a natural one. The natural transition was also observed in the study by Solís-Gallego et al. (2020) for the FX 63-137 airfoil at low Reynolds numbers.

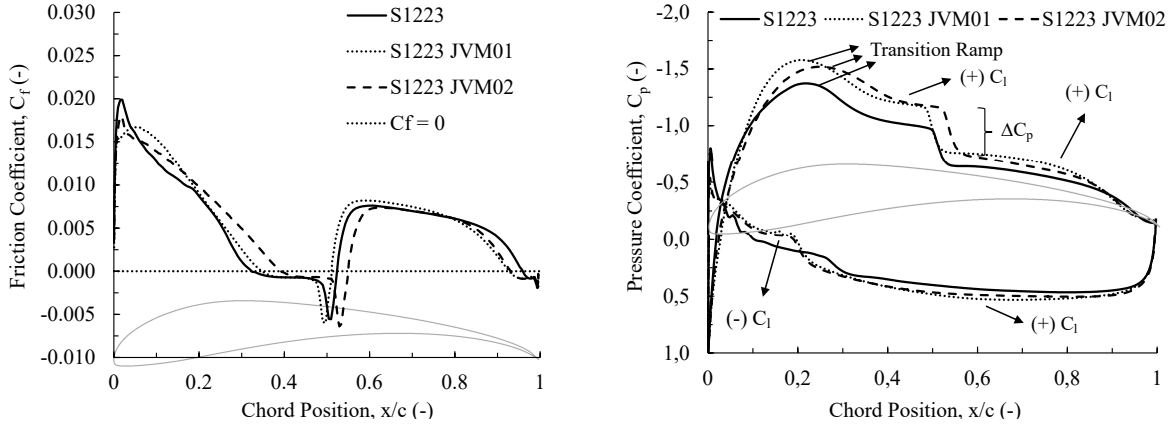

(a) C_f on the upper surface and the LSB region (b) Distribution of the C_p over the airfoil surface

Figure 9: Distribution of the pressure coefficient C_p and friction C_f coefficient on the airfoil surface.

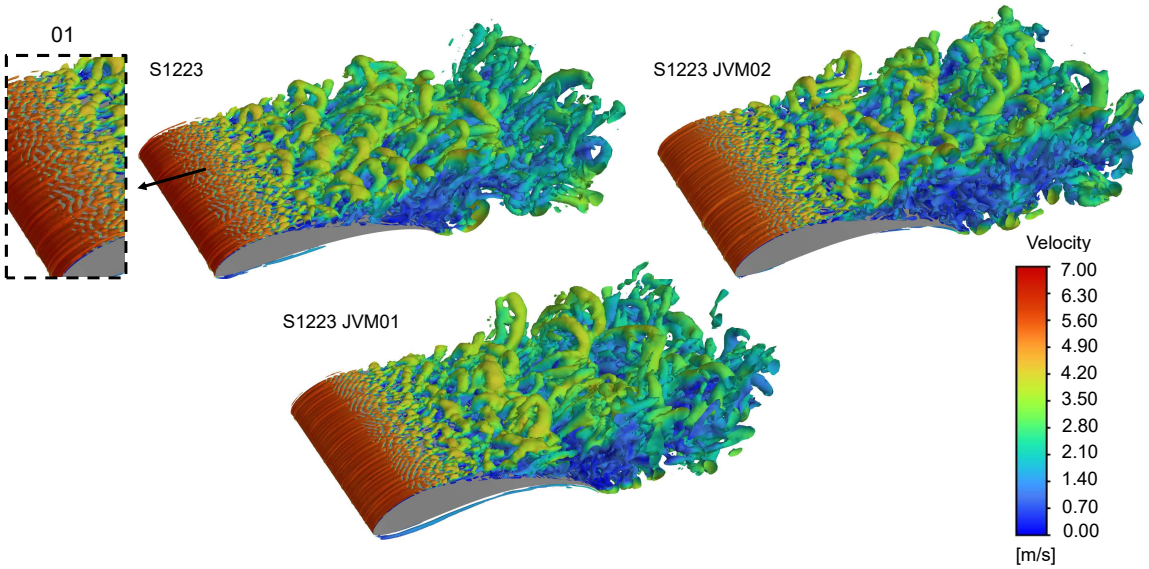

Figure 10: Isosurface Q = 300 for $\alpha = 18°$ using velocity contour.

4. CONCLUSIONS

This study developed airfoils using inverse design based on S1223, aiming to increase lift for low Reynolds number applications that require high lift capability. It was shown that further lift improvement is possible, even if it may be associated with additional drag. It was also demonstrated that increased lift can be achieved through greater curvature and thickness, maximizing the area under the pressure distribution curve, while stall and adverse effects are controlled through the transition ramp and adverse pressure gradient on the pressure recovery surface. In this context, it was observed that increased thickness combined with transition control can help mitigate adverse stall effects, maintaining the same stall angle of the S1223 airfoil for the S1223 JVM01 airfoil. The S1223 JVM02 airfoil, on the other hand, exhibited a smaller increase in drag (due to the different position of the pressure recovery) for a practically equal lift gain compared to the S1223 JVM01, despite having a lower stall angle. Both developed airfoils achieved significant lift gains (up to 15%) across the entire range and higher maximum lift coefficients, while maintaining stall characteristics and fulfilling the objectives of single-objective optimization. It was also observed that low Reynolds number airfoils are highly sensitive to transition aspects, highlighting the importance of considering this aspect in turbulence modeling, such as using the Transition SST model. The hybrid URANS/LES model, combined with Transition SST and the three-dimensional methodology, enhanced the prediction of aerodynamic coefficients, especially in the stall region due to the more complex flow.

5. REFERENCES

Ansys, I., 2021. *Ansys Fluent Theory Guide*. ANSYS Inc, Canonsburg, PA, release 2021 r2 edition.
Anyoji, M., Nonomura, T., Aono, H., Oyama, A., Fujii, K., Nagai, H. and Asai, K., 2014. “Computational and experimental

analysis of a high-performance airfoil under low-reynolds-number flow condition". *Journal of Aircraft*, Vol. 51, No. 6, pp. 1864–1871.

Ashby, D.L., 1996. "Experimental and computational investigation of lift-enhancing tabs on a multi-element airfoil". In *NASA Technical Memorandum 110432*. NASA, Ames Research Center - Moffett Field, California.

Boughou, S., Omar, A.A., Elsyed, O.A. and Aldheeb, M., 2022. "Numerical investigations of aerodynamic characteristics prediction of high-lift low reynolds number airfoil". *CFD Letters*, Vol. 14, pp. 111–121.

Cerra, D.F. and Katz, J., 2008. "Design and evaluation of a high-lift, thick airfoil for UAV applications". In *46th AIAA Aerospace Sciences Meeting and Exhibit*. Nevada, pp. 1–10.

da Silveira Neto, A., 2020. *Escoamentos turbulentos: Análise física e modelagem teórica*. Composer, Uberlândia, 1st edition.

de Medeiros Neto, M.P., 2016. *Veículos Aéreos Não Tripulados e Sistema de Entrega: Estudo, Desenvolvimento e Testes*. Mestrado em sistemas e computação, Universidade Federal do Rio Grande do Norte, Rio Grande do Norte.

Drela, M., 1988. "Low-reynolds-number airfoil design for the M.I.T. daedalus prototype: A case study". *Journal of Aircraft*, Vol. 25, No. 8, pp. 724 – 732.

Drela, M., 1989. "XFOIL: An analysis and design system for low reynolds number airfoils". *Low Reynolds Number Aerodynamics*, Vol. 54, pp. 1–12.

Echavarria, C., Hoyos, J.D., Jimenez, J.H., Suarez, G. and Saldarriaga, A., 2022. "Optimal airfoil design through particle swarm optimization fed by CFD and XFOIL". *Journal of the Brazilian Society of Mechanical Sciences and Engineering*, Vol. 44, No. 561, pp. 1–17.

Eppler, R., 1990. *Airfoil Design and Data*. Springer-Verlag Berlin Heidelberg GmbH, New York, 1st edition.

Hubbe, G.B.B., 2017. *NUMERICAL AND EXPERIMENTAL ANALYSIS OF A HIGH LIFTING AIRFOIL AT LOW REYNOLDS NUMBER FLOWS*. Mestrado em engenharia mecânica, Universidade Federal de Santa Catarina, Florianópolis.

Liebeck, R.H., 1978. "Design of subsonic airfoils for high lift". *AIAA Journal*, Vol. 15, No. 9, pp. 547 – 561.

Ma, R. and Liu, P., 2009. "Numerical simulation of low-reynolds-number and high-lift airfoil s1223". In *Proceedings of the World Congress on Engineering 2009*. London, pp. 1–6.

Ma, R., Zhong, B., Liu, P. and Drikakis, D., 2010. "Multi-objective optimization design of low-reynolds-number airfoils s1223". In *27TH INTERNATIONAL CONGRESS OF THE AERONAUTICAL SCIENCES*. pp. 1–10.

Menter, F.R., 2015. *Best Practice: Scale-Resolving Simulations in ANSYS CFD*. Ansys Germany GmbH, Germany, 2nd edition.

Mereu, R., Passoni, S. and Inzoli, F., 2019. "Scale-resolving CFD modeling of a thick wind turbine airfoil with application of vortex generators: Validation and sensitivity analyses". *Journal of Energy*, Vol. 187, No. 115969, pp. 1 – 15.

Morgan, H.L. and Ferris, J.C., 1987. "A study of high-lift airfoils at high reynolds numbers in the langley low-turbulence pressure tunnel". In *NASA Technical Memorandum 89125*. NASA, Langley Research Center - Hampton, Virginia.

Nwokolo, E., Agboola, O., Olatoyinbo, S.F., Yusuf, O.T., Olukunle, S.K. and Iliya, S.Z., 2023. "Optimization of low reynolds number airfoil design using full inverse design method". *Research Square*.

Sa, J.H., Cho, K.W. and Park, S.H., 2016. "Numerical study of blending hybrid RANS/LES method and $\gamma - Re_\theta$ transition model for unsteady turbulent flow analysis". In *The 2016 Structures Congress*. pp. 1–8.

Selig, M.S., 2003. *Low Reynolds Number Airfoil Design Lecture Notes*. von Karman Institute for Fluid Dynamics, Illinois, USA.

Selig, M.S. and Guglielmo, J.J., 1997. "High-lift low reynolds number airfoil design". *Journal of Aircraft*, Vol. 34, pp. 73 – 79.

Selig, M.S., Guglielmo, J.J., Broeren, A.P. and Giguère, P., 1995. *Summary of Low-Speed Airfoil Data*. SoarTech Publications, Virginia, 1st edition.

Solís-Gallego, I., Díaz, K.M.A., Oro, J.M.F. and Velarde-Suárez, S., 2020. "Wall-resolved LES modeling of a wind turbine airfoil at different angles of attack". *Journal of Marine Science and Engineering*, Vol. 8, No. 212, pp. 1 – 18.

Wang, Y., Liu, K., Song, W. and Han, Z., 2019. "Scale adaptive simulations of unsteady flow around NACA0021 airfoil at 60° angle of at 60° angle of attack". *American Institute of Aeronautics and Astronautics*, Vol. 187, No. 115969, pp. 1 – 15.

Wauters, J. and Degroote, J., 2018. "On the study of transitional low-reynolds number flows over airfoils operating at high angles of attack and their prediction using transitional turbulence models". *Progress in Aerospace Sciences*, Vol. 103, pp. 52–68.

Wei, X., Wang, X. and Chen, S., 2020. "Research on parameterization and optimization procedure of low-reynolds number airfoils based on genetic algorithm and bezier curve". *Advances in Engineering Software*, Vol. 149, No. 102864, pp. 1–12.

6. RESPONSIBILITY NOTICE

The authors are solely responsible for the printed material included in this paper.